Quantum Criticality of Generalized Aubry-André Models with Exact Mobility Edges Using Fidelity Susceptibility

Yu-Bin Liu, 1,2,* Wen-Yi Zhang, 1,2,* Tian-Cheng Yi, Liangsheng Li, Maoxin Liu, and Wen-Long You, t

¹College of Physics, Nanjing University of Aeronautics and Astronautics, Nanjing, 211106, China

²Key Laboratory of Aerospace Information Materials and Physics (NUAA), MIIT, Nanjing 211106, China

³Department of physics, Zhejiang Sci-Tech University, Hangzhou 310018, China

⁴National Key Laboratory of Scattering and Radiation, Beijing 100854, China

⁵School of Systems Science & Institute of Nonequilibrium Systems, Beijing Normal University, Beijing 100875, China

In this study, we explore the quantum critical phenomena in generalized Aubry-André models, with a particular focus on the scaling behavior at various filling states. Our approach involves using quantum fidelity susceptibility to precisely identify the mobility edges in these systems. Through a finite-size scaling analysis of the fidelity susceptibility, we are able to determine both the correlation-length critical exponent and the dynamical critical exponent at the critical point of the generalized Aubry-André model. Based on the Diophantine equation conjecture, we can determines the number of subsequences of the Fibonacci sequence and the corresponding scaling functions for a specific filling fraction, as well as the universality class. Our findings demonstrate the effectiveness of employing the generalized fidelity susceptibility for the analysis of unconventional quantum criticality and the associated universal information of quasiperiodic systems in cutting-edge quantum simulation experiments.

I. INTRODUCTION

In past decades, the study of phase transitions in disordered systems has gained upsurging interest in condensed matter physics. Anderson's pioneering theory of localization in noninteracting disordered systems has achieved remarkable success [1]. Such systems may exhibit many-body localization (MBL) in the presence of many-body interactions [2]. Recently, the phenomenon of MBL was investigated extensively from both theoretical and experimental perspectives [3–5]. A key insight of current phenomenological theory is that MBL systems exist an emergent integrability, which is characterized by a set of quasilocal integrals of motion. The emergent integrability plays a similar role of exact integrability in integral systems, and leads to a breakdown of thermalization in isolated systems. Interestingly, the strong ergodicity breaking arising from integrability and disorder fails to describe the recent discovery of quantum many-body scars, which triggered intensive investigations of weak ergodicity breaking in a variety of quantum systems [6–8]. Compelling theoretical and numerical evidence suggests the phenomenon of localization and non-ergodicity can exist in quasiperiodic models. Compared to random disorder, which poses challenges in experimental engineering [9], incommensurate potential systems are more accessible for experimental platforms, particularly in the context of ultra-cold atoms [10], photonic crystals [11] and cavity polaritons [12, 13], providing a fertile ground for investigating incommensurate potential driven localization. The dispensation of disorder averaging has conduced to an in-depth theoretical investigations in quasiperiodic systems. Despite many physical features in common, such as multifractal wave functions and exponentially-diverging localization length, the critical properties of the localization transition in random and incommensurate models are rather different. As the random matrix theory is not applicable to describing incommensurate models [14], there are no rigorous bounds on the critical exponents concerning the localization transition [15]. Considering all eigenstates of Anderson model will be localized for an infinitesimal disorder strength in one and two dimensions (1D, 2D), a distinct feature of incommensurate model is the access to a localization-delocalization transition in 1D. Therefore, quasiperiodic models open the door to effectively simulate some properties of Anderson localization that occur generically in three dimensions (3D) and offer a fascinating platform to explore unconventional phenomena, including fractal bands [16, 17], mobility edge (ME) [18], Bose glass [19], topological phases [20], and non-Hermitian Floquet quasicrystals [21].

Among a diversity of quasiperiodic models, the Aubry-André (AA) model and its generalizations are drawing increasing attention nowadays due to its experimental realizations [22, 23]. The 1D AA model was originally derived from the reduction of a square-lattice Hofstadter Hamiltonian describing conduction electrons in the presence of a uniform magnetic field [24]. A dual transformation between the coordinate and momentum spaces will yield the same Hamiltonian with hopping and potential amplitudes interchanged. As a consequence of the inherent self-duality, all the eigenstates of the system undergo Anderson localization transition from an extended phase (EP) to a localized phase (LP) at a critical value of the incommensurate potential strength [25, 26]. At the transition, the energy spectrum showcases the renowned Hofstadter butterfly pattern [27]. The multifractal gap structure that ultimately evolves into the localization of the particles above the transition point. During the past few years, inspiring progress is made by tailoring the incommensurate potential to introduce a single-particle ME into the AA model [28], which separates localized and delocalized eigenstates at a critical energy. Typical variants encompass slowly varying Aubry-André model [29, 30], mosaic Aubry-André model [31] and generalized Aubry-André model (GAA) [32].

^{*} These authors contributed equally to this work.

[†] wlyou@nuaa.edu.cn

Motivated by the recent experimental progress, specifically the successful simulation of the GAA model by using quantum Cs gas [33] and using synthetic lattices of laser-coupled atomic momentum modes [34], we consider critical properties of the GAA model that has a single-particle ME at a finite filling. Our primary focus is on the scaling behavior of the fidelity susceptibility across the localization transition between the EP and the EP at different filling fractions. In the context of the Widom scaling hypothesis [35], which is foundational to the field of critical phenomena, it is posited that a complete characterization of a universality class of a phase transition can be achieved using just two independent critical exponents. The finite-size scaling of the generalized participation indicated that the correlation-length critical exponent $\nu = 1$ for the AA model, in which an incommensurate on-site potential is characterized by an irrational number α . A second independent critical exponent thus plays a decisive role in determining the universality class. The ground state universality class of quasiperiodic models has been thoroughly investigated using a renormalization group scheme [36, 37]. It has been recognized that the universality class of the ground state depended solely on the continued-fraction expansion of α [38]. Furthermore, the dynamic critical exponent z exhibits a significant dependence on irrational numbers. The value of zat different filling fractions dictate the scaling behavior of the corresponding energy spectrum [39-41], which proves valuable in comprehending both the multifractal characteristics of the system [42] and the properties associated with multiparticle ground-state transitions. Notably, the relationship between z, α , and the filling fractions ρ is less thoroughly understood. A strategy using generalized fidelity susceptibility (GFS) to obtain the dynamical exponent z has been developed for the lowest state in the both CP-LP [43] and EP-CP transitions [44] of the p-wave-paired AA model.

This paper is organized as follows. In Sec. II, we briefly present the GAA models and the phase diagram. In Sec. III, we show the ME of GAA model by inverse participation ratio and fidelity susceptibility. In Sec. IV, we review the scaling hypothesis of fidelity susceptibility and present the numerical results of the critical behaviour in the GAA model. We also unravel the relationship between the Diophantine equation and the filling fractions. The summary and conclusion are given in Sec. V.

II. MODEL HAMILTONIAN

We consider a family of GAA models described by the following Hamiltonian

$$\hat{H} = -t \sum_{j=1}^{N} (\hat{c}_{j}^{\dagger} \hat{c}_{j+1} + \hat{c}_{j+1}^{\dagger} \hat{c}_{j}) + \sum_{j=1}^{N} V_{j} \hat{c}_{j}^{\dagger} \hat{c}_{j}, \tag{1}$$

in which the operator c_j^{\dagger} (c_j) represents the creation (annihilation) operator at site j among total N lattice sites, and the hopping amplitude t is set to be the unit energy scale, i.e., t=1. The on-site potential V_j is characterized by a modulation strength V, a wave number α , a deformation parameter b

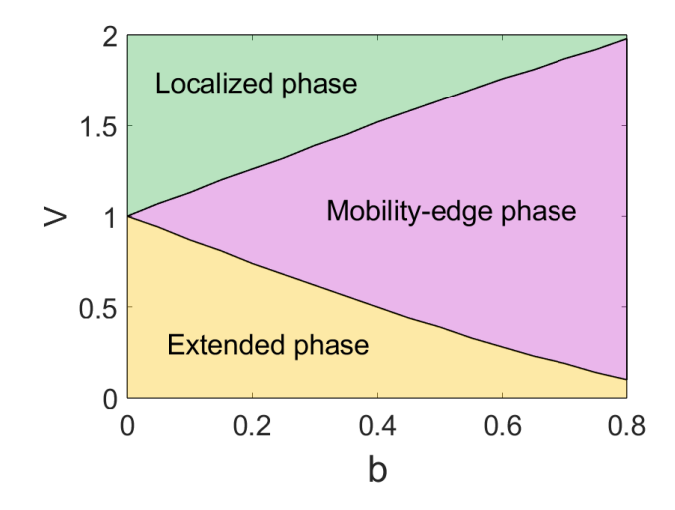


FIG. 1. Phase diagram of the GAA model as a function of the incommensurate potential strength V and the deformation parameter b. The green, yellow and pink regions represent the completely localized, completely extended and mobility-edge phases, respectively. In the mobility-edge phase, the extended states and localized states coexist. Here we choose N=1597.

and a random phase ϕ , given by

$$V_j = 2V \frac{\cos(2\pi\alpha j + \phi)}{1 - b\cos(2\pi\alpha j + \phi)}.$$
 (2)

When α takes an irrational value, the modulation becomes quasi-periodic. In this work, we employ $\alpha = (\sqrt{5} - 1)/2$. The on-site potential is a continuous function of the parameter b, where $b \in [0,1)$. When b = 0, the model (1) reduces to the standard AA model. For V < t all the single-particle eigenstates are extended, while they become localized simultaneity for V > t. At V = t, the system undergoes the Anderson localization transition, leading to all eigenstates becoming critical and exhibiting multifractal behavior. This localization transition at V = t is a consequence of a self-dual symmetry present in the system, which indicates the absence of the ME within the system. For $b \neq 0$, the deformed AA Hamiltonian in Eq. (1) respects an energy-dependent duality symmetry, which ensures the existence of localization transition. The GAA duality warrants the occurrence of the ME described by a closed-form analytical expression:

$$bE = 2(t - V), (3)$$

where E represents the single-particle energy. According to Eq. (3), we depict the phase diagram in Fig. 1, in which the single-particle eigenstates are categorized into three types: completely localized, completely extended and mobility-edge phases. In particular, low-energy states are extended in the mobility-edge phase. In this study, we investigate the phase transition from extended eigenstates to localized eigenstates by varying the filling fractions, denoted as $\rho = n/N$, in the mobility-edge phase, where n represents the index of the highest occupied eigenstate by fermions.

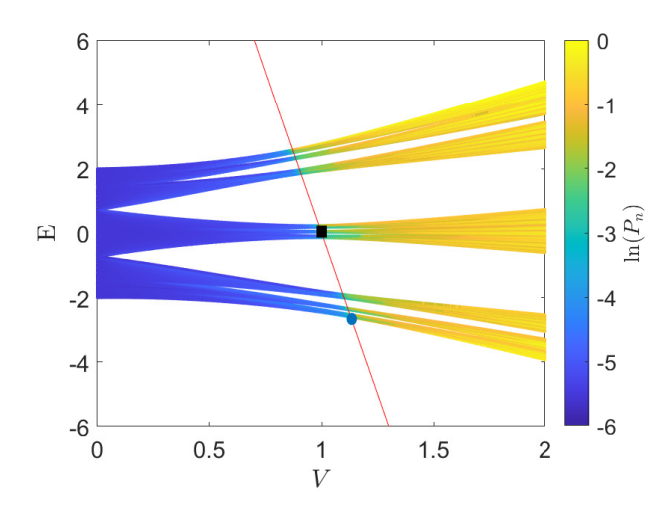


FIG. 2. The eigenvalues of Eq. (1) and IPRs as functions of the incommensurate potential strength V with deformation parameter b=0.1 and system size N=1597. The eigenvalue curves are color-coded to represent the varying magnitudes of the logarithmic IPR of their corresponding wave functions. The red line delineates the self-dual mobility edge as described in Eq. (3), marking the threshold where the energy-dependent localization transition occurs. Two symbols, black square and the blue circle, highlight the fermion numbers at $n=\lfloor N/2 \rfloor$ and n=1, respectively, to illustrate the scaling behaviors at these specific fillings in the following.

III. LOCALIZED TRANSITION OF GAA MODEL WITH EXACT MOBILITY EDGES

In order to obtain the eigenenergies of the system and the associated eigenstates on a finite lattice containing N sites, we numerically diagonalize the model Hamiltonian in Eq. (1). We impose antiperiodic boundary conditions to alleviate the boundary effects [45, 46]. In the actual numerical calculations, it is wise to replace the inverse golden ratio with a rational approximant being F_{k-1}/F_k , which will approach the inverse golden ratio for $k \to \infty$, i.e., $\alpha = \lim_{k\to\infty} F_{k-1}/F_k$. Here F_k represents the k-th Fibonacci number, which is recursively defined by $F_{k+1} = F_k + F_{k-1}$, with $F_0 = F_1 = 1$. The Fibonacci sequence, F_k , demonstrates a three-cycle parity pattern: odd, odd, even. As a result, the sequence is partitioned into three distinct subsequences, $\{F_{3l+1}|\cdots,55,233,987,\cdots\}$, $\{F_{3l+2}|\cdots,89,377,1597,\cdots\}$, $\{F_{3l+3}|\cdots,144,610,2584,\cdots\}$.

At the k-th rational approximation, the GAA potential and the Schrödinger equation have a periodicity of F_k sites, allowing for experimental realizations with available laser wavelengths. Then, it is convenient to calculate the physical quantities of interest on finite lattices. The eigenspectra and eigenstates can be determined by solving the Schrödinger equation

$$\hat{H}|\Psi_n\rangle = E_n|\Psi_n\rangle,\tag{4}$$

where $|\Psi_n\rangle = \sum_j \psi_{n,j} |j\rangle$ expressed in terms of Wannier basis $|j\rangle$, representing the state of a single particle localized at

the site j of the lattice. The Hamiltonian (1) can be recast into

$$\hat{H} = \hat{\mathbf{c}}^{\dagger} \mathcal{H} \hat{\mathbf{c}},\tag{5}$$

where $\hat{\mathbf{c}} = [\hat{c}_1, \cdots, \hat{c}_{F_k}]^T$ and \mathcal{H} is a $F_k \times F_k$ single-particle Hamiltonian matrix, given by

$$\mathcal{H} = \begin{pmatrix} V_{1} & -t & 0 & \cdots & \cdots & \cdots & t \\ -t & V_{2} & -t & 0 & \cdots & \cdots & 0 \\ 0 & -t & V_{3} & -t & \ddots & \ddots & 0 \\ \vdots & \ddots & \ddots & \ddots & \ddots & \ddots & \vdots \\ 0 & \cdots & 0 & -t & V_{F_{k}-2} & -t & 0 \\ 0 & \cdots & \cdots & 0 & -t & V_{F_{k}-1} & -t \\ t & \cdots & \cdots & \cdots & -t & V_{F_{k}} \end{pmatrix}.$$
 (6)

In order to visually characterize the localized and extended nature of the entire energy spectrum, we evaluate the normalized inverse participation ratio (IPR) for n-th eigenstate $|\Psi_n\rangle$ of the model (1), given by [47–49]

$$P_n = \frac{\sum_{j=1}^{N} |\psi_{n,j}|^4}{(\sum_{j=1}^{N} |\psi_{n,j}^2|)^2}.$$
 (7)

The IPRs can quantify the extent of distribution over the Fock space. For a set of single-particle states in real space, the IPR scales inversely with the system size N in extended states, while appears to be independent of N in the localized states. We plot the logarithm of normalized IPR for all eigenmodes of Eq. (1) as functions of V with the deformation parameter b=0.1 in Fig. 2. Hereafter, unless otherwise specified, we set b=0.1. The localization transition from the EP to the LP occurs at mobility edges in Eq. (3). In the following, our primary emphasis will be on two specific cases: one where the fermion number is $n=\lfloor N/2 \rfloor$, corresponding to a filling fraction of $\rho=1/2$, and another where the fermion number is n=1, corresponding to a filling fraction of $\rho=1/N$. Here $\lfloor \cdot \rfloor$ denotes the round function.

As the IPR is bounded, it is not easy to accurately identify the critical point, as is revealed in Fig. 3(a). Here we use quantum fidelity susceptibility (QFS) as a versatile indicator of localization transition points. The fidelity susceptibility quantifies the sensitivity of an eigenstate to variations of the driving parameter, which is defined as the second-order derivative of the quantum fidelity with respect to the driving parameter [50]. Being a purely geometric measure, the fidelity approach offers a notable advantage by not requiring any prior knowledge of the order parameter. A GFS of order 2r+2 associated with the eigenstate $|\Psi_n\rangle$ with the tuning parameter V is given by [51]

$$\chi_{2r+2}^{(n)} = \sum_{m \neq n} \frac{|\langle \Psi_m | \partial_V \hat{H} | \Psi_n \rangle|^2}{(E_m - E_n)^{2r+2}}.$$
 (8)

The numerator in Eq.(8) denotes the probability of exciting the system away from the state $|\Psi_n\rangle$ through a relevant (or marginal) perturbation $\partial_V \hat{H}$. The GFS of different orders is encoded by the power of the denominator. For the case of

r=-1/2, Eq. (8) simplifies to the second derivative of the eigenenergy [52], denoted as $\chi_1^{(n)}\equiv\partial^2 E_n/\partial V^2$. Similarly, when r=0, Eq. (8) reverts to the QFS, i.e., $\chi_2^{(n)}\equiv\partial^2(1-F)/\partial V^2$, where the fidelity F is defined as the absolute value of the inner product between $|\Psi_n(V)\rangle$ and $|\Psi_n(V+\delta V)\rangle$. This fidelity quantifies the Bures distance between two states as their tuning parameter slightly changes.In the following, we focus on the GFS of the eigenstate $|\Psi_n(V)\rangle$ at a finite filling fraction for $n=\lfloor \rho F_k \rfloor$, where $\lfloor x \rfloor$ rounds x to the nearest integer. To this end, the superscript of $\chi_{2r+2}^{(n)}$ is omitted for abbreviation.

Different from the smooth transition of the IPR around the mobility edge, the QFS shows a divergent peak in the vicinity of the EP-LP transition point due to the enhanced sensitivity, as is disclosed in Fig. 3(b). The QFS and GFS have been widely used to witness the quantum phase transitions in quantum systems [53] and even holographic models [54, 55]. They have proved to be particularly useful for detecting the critical points of a symmetry-knowledge unknown systems [56–58]. It has been demonstrated that the QFS not only facilitates the identification of quantum critical points (QCPs) but also adheres to the scaling ansatz, enabling the retrieval of critical exponents. The retrieved critical exponents conform to the hyperscaling relations, signifying the existence of only two independent exponents. The key implication is that the finitesize scaling behavior of the standard fidelity susceptibility χ_2 determines the positions of QCP, along with the correlationlength critical exponent ν associated. Notably, a second critical exponent assumes a pivotal role in establishing the universality class such as the dynamical exponent z. In the context of quasiperiodic systems exhibiting spatial complexity, the scaling behavior of the QFS and the universality class of the localization transition have received relatively less exploration. Specifically, we are able to extract two critical exponents and universal information by observing the finite-size scaling of the GFS, which is particularly remarkable considering the constraints posed by the limited number of system sizes available within quasiperiodic systems.

IV. SCALING BEHAVIOR AND DIOPHANTINE EQUATION

The finite-size scaling theory of GFS is applicable in the vicinity of continuous quantum phase transitions, as the sensitivity is much more pronounced for the GFS around the QCP than that away from criticality [59]. When V is adiabatically crossed over the QCPs V_c , the GFS of a finite system displays a peak, effectively indicating the positions of pseudocritical points V_m . With increasing system sizes N, the peaks of the GFS become more prominent. Additionally, it is anticipated that the maximal value of the GFS is expected to obey a power-law relation with the system size as [51]

$$\chi_{2r+2}(V_m) \sim N^{-\mu},$$
(9)

where $\mu=2/\nu+2zr$ corresponds to the critical adiabatic dimension. Here, ν denotes the correlation-length exponent,

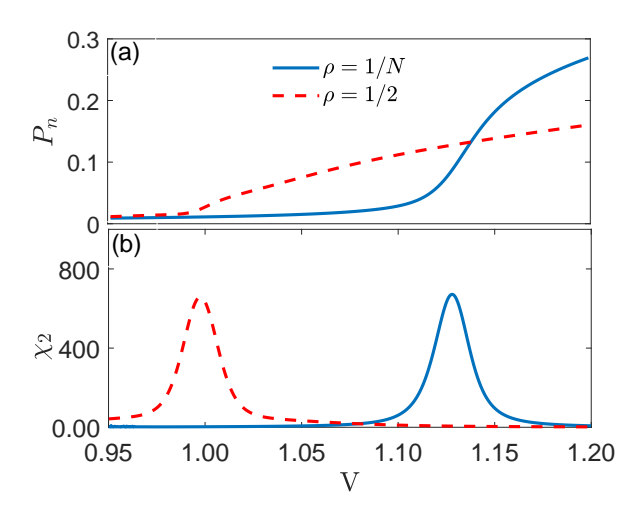


FIG. 3. (a) IPRs and (b) QFS as a function of the incommensurate potential strength V for different filling fractions: $\rho=1/2$ (red dashed lines) and $\rho=1/N$ (blue dashed lines). Here we choose the deformation parameter b=0.1, phase $\phi=\pi$ and the lattice site N=377.

and z represents the dynamical critical exponent. According to single-parameter scaling theory, the correlation length ξ becomes the only relevant length scale in the thermodynamic limit that diverges near the phase transition as [60],

$$\xi \sim |V - V_c|^{-\nu},\tag{10}$$

and the single-particle spectral gap ϵ_s is predicted to close following the relation

$$\epsilon_s \sim N^{-z}$$
. (11)

For a relevant operator such as $\partial_V \hat{H}$ applied to sufficiently large one-dimensional systems, where $\nu < 2$, the pseudocritical points V_m tend to approach the critical points V_c , thereby satisfying

$$|V_m - V_c| \propto N^{-1/\nu}.\tag{12}$$

Consequently, the GFS of a finite system with size N in the vicinity of a QCP shall obey a universal scaling form [61],

$$\chi_{2r+2}(V) = N^{2/\nu + 2zr} \phi_r(|V - V_m| N^{1/\nu}).$$
 (13)

Here, $\phi_r(x)$ represents a unknown regular universal scaling function for the GFS of order 2r+2. In this case, estimates for critical parameters can be deduced by plotting the scaled GFS as $[\chi_{2r+2}(V_m)-\chi_{2r+2}(V)]/\chi_{2r+2}$ against $N^{1/\nu}(V-V_m)$, with subtle adjustments made to the values of V_m , ν , and z until achieving a collapse of data.

Figure 4 shows the logarithm of the GFS, including $\ln\chi_2$ and $\ln\chi_4$ of the GAA model, as a function of V for various system sizes N with $\phi=\pi$. We observe that χ_4 exhibits a much more pronounced divergence compared to χ_2 at a critical point, yet there exist distinctions between the cases of $\rho=1/N$ and $\rho=1/2$. The logarithmically scaled maximum values of the GFS, $\chi_{2,\mathrm{max}}$ and $\chi_{4,\mathrm{max}}$, in proximity to

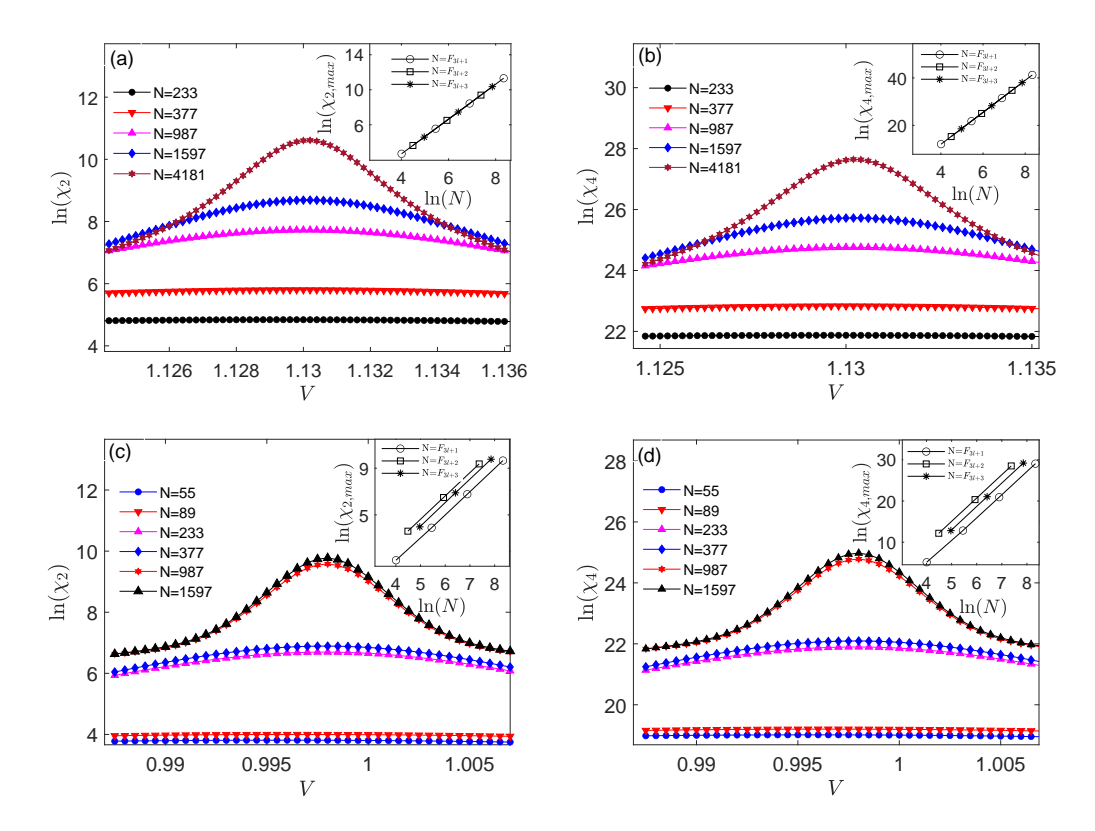


FIG. 4. The GFS in the GAA model with deformation parameter b=0.1 and phase $\phi=\pi$. (a) The logarithm of the second-order GFS χ_2 and (b) the fourth-order GFS χ_4 as functions of the incommensurate potential strength V for various lattice sizes at a filling fraction of $\rho=1/N$. Panels (c) and (d) similarly depict χ_2 and χ_4 , respectively, at a filling fraction of $\rho=1/2$. The insets in each panel illustrate the scaling behavior of the peak maxima for system sizes represented by Fibonacci sequences $N=\{F_{3l+1}|55,233,987\}, \{F_{3l+2}|89,377,1597\}$ and $\{F_{3l+3}|144,610,2584\}$.

the QCP are plotted against various system sizes N, which confirm the linear scaling relations by the numerical fittings. In-depth analysis of the insets in Figs. 4(a) and (b) reveals interesting behavior regarding the filling fraction $\rho = 1/N$. Specifically, at this fraction, only a single subsequence is apparent. However, an interesting deviation occurs for even subsequences compared to odd ones when the phase ϕ is set to 0. To mitigate this odd-even effect and ensure consistent data analysis, we appropriately adjust the value of ϕ to π , thereby aligning the subsequences more uniformly. According to Eq. (13), the linear fitting for various system sizes N gives rise to $\nu = 0.998 \pm 0.0015$ and $z = 2.3705 \pm 0.0025$, while the numerical fitting for even number of system sizes N yields $\nu = 0.998 \pm 0.009$ and $z = 2.371 \pm 0.018$. On the contrary, when considering $\rho = 1/2$, the numerical result reveals a division of the sequence into three distinct subsequences for numerous values of ϕ . As shown in the inset of Fig. 4(c), the linear fittings of the log-log plot give rise to $\nu = 1.004 \pm 0.0515$ for $N = F_{3l+1}$, $\nu = 0.9985 \pm 0.0030$ for $N = F_{3l+2}$ and $\nu = 1.0005 \pm 0.0015$ for $N = F_{3l+3}$. Likewise, from the inset of Fig. 4(d), the dynamical exponent can be fitted as $z = 1.8265 \pm 0.0082$ for $N = F_{3l+1}$, $z = 1.8305 \pm 0.0138$ for $N = F_{3l+2}$ and $z = 1.8355 \pm 0.078$ for $N = F_{3l+3}$. By calculating their averages, we determine the correlationlength critical exponent of $\nu = 1.001 \pm 0.0186$ and the dynamical critical exponent of $z=1.83083\pm0.03332$ for the filling fraction $\rho=1/2$.

Recent studies have highlighted an intimate relation between finite-size effects and Diophantine equation in the AA model [46]. The solutions of the Diophantine equation, obtained through continued fraction expansions, elucidate a mathematical framework that captures the essence of the system's quasi-periodicity, which is fundamental to understanding its renormalization group dynamics [36]. The Diophantine equation establishes a link between the filling fraction and the disorder's incommensurate frequency, refining the resonance criterion $Q\alpha - P = \rho$ of commensurate cases [62], where Q and P are integers that do not exceed the system size N. This association is based on the continued-fraction expansion of the frequency α . When Q and P remain fixed irrespective of system size, and the resonance equation is solved precisely, the system is deemed commensurate. In this state, Q determines the perturbation order where the resonance between the Fermi momentum and the potential frequency α occurs. Conversely, when Q and P scale with the system size, the system is recognized as incommensurate. Under these circumstances, the resonance criterion transcends into a Diophantine equation requiring a solution that accommodates the scaling variables, which then forms the mathematical foundation for understanding the resonance phenomena within the incommensurate framework. The incommensurate filling ρ , marked by the growth of Q and P with system size N, implies a dynamic interplay between the system's physical dimensions and its spectral properties. This Diophantine equation not only serves as a tool for solving for these properties but also encapsulates the essence of the incommensurate state within the GAA model. Our investigation focuses on exploring this relationship further within the GAA model, particularly examining the sequence effects.

We note that α can be approximated by $\alpha_k = F_{k-1}/F_k$ and $n = \lfloor \rho F_k \rfloor$. Consequently, the Diophantine equation is reformulated as

$$Q_k F_{k-1} - P_k F_k = \pm n, (14)$$

To seek integer solutions (Q_k, P_k) for given integer values of F_k and n. For each value of k, an infinite spectrum of solutions (Q_k, P_k) hat satisfy the resonance condition in Eq. (14). The solutions are constrained to $|Q_k| \leq F_k/2$,and among these, the smallest $|Q_k|$ is selected. When solving the Diophantine equation for different values of F_k and n, the ratio $|Q_k|/F_k$ for large k displays a periodicity of p distinct values, thus dividing the sequence of denominators into p subsequences. As illustrated in Table I, p also corresponds to the number of scaling functions, such as p=1 for $\rho=1/N$ and p=3 for $\rho=1/2$ at half filling. Further details are available in Appendix A.

ρ	0	0.25	0.5	p
1/N		2.3740 ± 0.0020		1
1/3		2.0046 ± 0.0090		4
	1.8285±0.0075			3
1	2.3740 ± 0.0020	2.3750 ± 0.0012	2.3735 ± 0.0010	1

TABLE I. The dynamical exponents z and numbers of sequences p extracted from finite-size scaling at various fillings. The number of scaling functions p is determined by scaling collapse as in Fig. 5 and via the Diophantine equation where it is determined by the period of the repeating values of $|Q_k|/F_k$ for large k.

The universality class, central to the study of critical phenomena, posits that associated critical exponents and scaling functions are universal, subject only to symmetries and space dimensionality. We validate the obtained critical exponents using the data collapse technique, as demonstrated in Fig. 5. The scaling hypothesis suggests that appropriately scaled curves can converge into a single unified curve. To facilitate this data collapse, we employ the rescaled fidelity susceptibility as defined in Eq.(13):

$$[\chi_2(V_m) - \chi_2(V)]/\chi_2(V) \sim \mathcal{F}_q(N^{1/\nu}\delta),$$
 (15)

where $\delta=V-V_m$ is the deviation from the pseudocritical point, and \mathcal{F}_q $(q=1,2,\cdots p)$ is scaling functions. Based on Eq. (15), we plot $\left[\chi_2(V_m)-\chi_2(V)\right]/\chi_2(V)$ versus $N^{1/\nu}(V-V_m)$ for different values of N as depicted in Fig.5. For $\rho=1/N$ all curves of distinct chain sizes in the vicinity of V_m collapse onto a single curve in Fig. 5 (a), while for $\rho=1/2$ the scaling of χ_2 collapses all the curves onto three

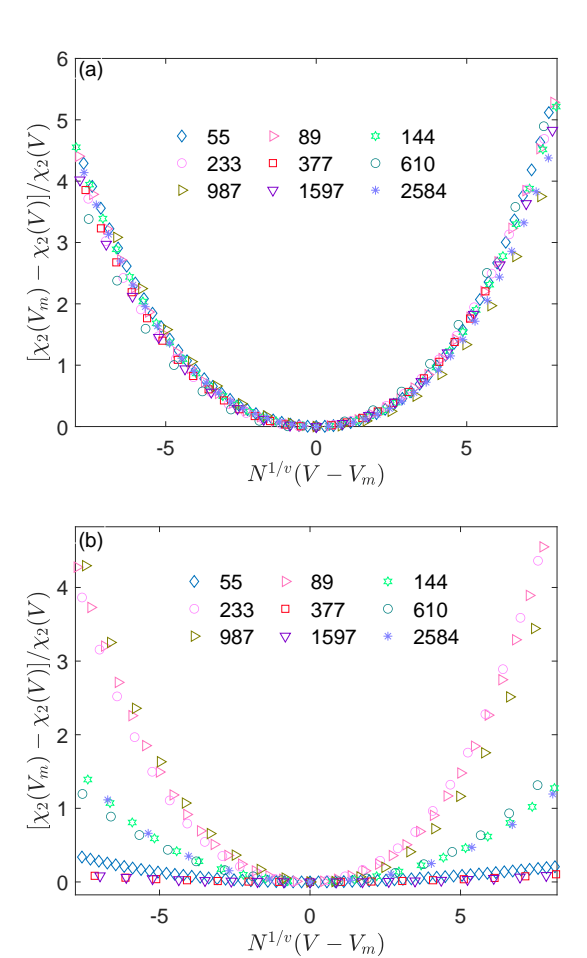


FIG. 5. Scaling analysis of the GFS in the GAA model. (a) Scaled fidelity susceptibility, calculated as $[\chi_{2r+2}(V_m)-\chi_{2r+2}(V)]/\chi_{2r+2},$ is plotted against the scaled variable $N^{1/\nu}(V-V_m)$ for a filling fraction of $\rho=1/N$. (b) A similar analysis is presented for a filling fraction of $\rho=1/2$, where the scaled fidelity susceptibility is plotted against the same scaled variable. Here we choose deformation parameter b=0.1, phase $\phi=\pi$ and the correlation-length critical exponent $\nu=1.000$.

scaling functions. A very good quality data collapse confirms that the scaling hypothesis is in place and the estimated value of V_c , ν , z obtained through the prescriptions in Eq.(9) and (12) are self-consistent.

Similar strategies are applicable across various filling fractions. Our main findings in this work are the numerical results of the dynamical exponent z for different filling ρ and various values of b, as summarized in Tab. I. We observe that the value of z and the number of scaling functions p are influenced by the filling fraction ρ , yet they remain independent of the deformation parameter b. As indicated in Tab.I, for a filling fraction of $\rho=1/N$, the dynamical critical exponent z is approximately 2.734. At $\rho=1/3$, z is around 2.00, and for $\rho=1/2$, z is approximately 1.825. Intriguingly, at $\rho=1$, despite the localization transition not occurring at the same critical points as in the case of $\rho=1/N$, a symmetry persists, and the dynamical critical exponent is approximately 2.734

in both scenarios. This consistency of the dynamical critical exponents across similar filling states under varying mobility edges demonstrates that the Diophantine equation is applicable to the AA model, even when self-duality is broken.

V. SUMMARY

In this study, we employ quantum fidelity susceptibility (QFS) to pinpoint the mobility edge in the Anderson localization transition. Recognized as a potent tool for probing quantum criticalities, the fidelity susceptibility has demonstrated its efficacy in one-dimensional disordered lattice models, as well as in the p-wave-paired Aubry-André-Harper model. Here our research thus focuses on the generalized Aubry-André (GAA) model, which is characterized by an exact mobility edge (ME) leading to a transition between the localized phase and the extended phase within its energy spectrum. A significant aspect of our approach involves utilizing generalized fidelity susceptibility (GFS) to deduce both the correlation-length critical exponent ν and the dynamical critical exponent z. A notable observation in our study is the manifestation of finite-size effects on the critical behavior of GFS. Furthermore, the number of scaling functions, denoted as p, conforms to the Diophantine equation, taking into account the varying filling fractions and system sizes. This led us to conduct extensive tests across different filling fractions and under diverse ME conditions, culminating in the derivation of the correlation-length and dynamical critical exponents, as shown in Table I. The recent experimental verification of the existence of MEs [33] underscores the timeliness and relevance of our theoretical approach. By elucidating the localization transformations and critical exponents in the GAA model via QFS, our work lays a robust theoretical foundation for understanding the underlying mechanisms of ME phenomena. In conclusion, this research makes a substantial contribution to the field of quantum physics, particularly in understanding phenomena like the localization transition, mobility edge, and critical behavior in quantum systems. It introduces novel analytical methodologies and provides theoretical insights that align closely with recent experimental findings, thus enriching the current scientific discourse in this domain.

ACKNOWLEDGMENTS

The authors appreciate very insightful discussions with Ting Lv. This work is supported by the National Natural Science Foundation of China (NSFC) under Grant No. 12174194, Postgraduate Research & Practice Innovation Program of Jiangsu Province, under Grant No. KYCX23_0347, Opening Fund of the Key Laboratory of Aerospace Information Materials and Physics (Nanjing University of Aeronautics and Astronautics), MIIT, Top-notch Academic Programs Project of Jiangsu Higher Education Institutions (TAPP), and stable supports for basic institute research under Grant No. 190101.

Appendix A: Number of scaling functions determined by the Diophantine equation

The universality class of the single-particle ground state is known to depend solely on the continued-fraction expansion of the wave vector α . This expansion can be expressed as

$$\alpha = \alpha_1 + \frac{1}{\alpha_2 + \frac{1}{\alpha_2 + \cdots}} = [\alpha_1, \alpha_2, \alpha_3, \cdots]. \tag{A1}$$

By truncating the series at α_k we obtain a rational approximation of α as $\alpha \approx M_k/N_k$, where M_k and N_k are coprime. Consequently the system sizes are considered to be N_k that satisfy (anti)periodic boundary conditions. Generally, two values of α are said to have the same asymptotic continuedfraction expansion if there exists a natural number k such that for all i > k, the n_i in their expansions are identical. The number of scaling functions p is determined by the scaling collapse of the GFS and also by the Diophantine equation. This is particularly influenced by the period of the repeating values of $q_k \equiv |Q_k|/N_k$ for large k, for specific values of the wave number α and the filling fraction ρ . For instance, the golden mean $\alpha = (\sqrt{5} + 1)/2 = [1, 1, 1, \cdots]$. The inverse of the golden mean is $\alpha = (\sqrt{5} - 1)/2 = [0, 1, 1, \cdots]$. Its rational approximations from the continued-fraction expansion are given by $\alpha \approx F_{k+1}/F_k$, where F_k are the Fibonacci numbers, defined by $F_1 = 1$, $F_2 = 1$, and $F_{k+1} = F_k + F_{k-1}$.

Considering a filling fraction the filling fraction $\rho=1/N$ (i.e., n=1), we can calculate Q_k and P_k for different system sizes F_k . The following equations present these calculations:

$$F_8 = 21, n = 1, Q_8 = 8, P_8 = 5, q_8 = 0.38095,$$

$$F_9 = 34, n = 1, Q_9 = 13, P_9 = 8, q_9 = 0.38235,$$

$$F_{10} = 55, n = 1, Q_{10} = 21, P_{10} = 13, q_1 = 0.38182,$$

$$F_{11} = 89, n = 1, Q_{11} = 34, P_{11} = 21, q_1 = 0.38202,$$

$$F_{12} = 144, n = 1, Q_{12} = 55, P_{12} = 34, q_1 = 0.38194,$$

$$F_{13} = 233, n = 1, Q_{13} = 89, P_{13} = 55, q_1 = 0.38197,$$

$$F_{14} = 377, n = 1, Q_{14} = 144, P_{14} = 89, q_1 = 0.38196,$$

$$F_{15} = 610, n = 1, Q_{15} = 233, P_{15} = 144, q_1 = 0.38197,$$

$$F_{16} = 987, n = 1, Q_{16} = 377, P_{16} = 233, q_1 = 0.38197,$$

$$F_{17} = 1597, n = 1, Q_{17} = 610, P_{17} = 377, q_1 = 0.38197.$$

It becomes apparent that the value of $|Q_k|/N_k$ for large k stabilizes with a period of p=1 in the case of $\rho=1/N$.

Now, considering the half filling, i.e., $\rho = 1/2$, we again determine Q_k and P_k for various system sizes F_k . The data is

presented as follows:

$$\begin{split} F_8 &= 21, n = 11, Q_8 = 4, P_8 = 3, q_8 = 0.19048, \\ F_9 &= 34, n = 17, Q_9 = 17, P_9 = 10, q_9 = 0.5, \\ F_{10} &= 55, n = 28, Q_{10} = 17, P_{10} = 10, q_2 = 0.30909, \\ F_{11} &= 89, n = 45, Q_{11} = 17, P_{11} = 10, q_3 = 0.19101, \\ F_{12} &= 144, n = 72, Q_{12} = 72, P_{12} = 44, q_4 = 0.5, \\ F_{13} &= 233, n = 117, Q_{13} = 72, P_{13} = 45, q_2 = 0.30901, \\ F_{14} &= 377, n = 189, Q_{14} = 72, P_{14} = 45, q_3 = 0.19098, \\ F_{15} &= 610, n = 305, Q_{15} = 305, P_{15} = 188, q_4 = 0.5, \\ F_{16} &= 987, n = 494, Q_{16} = 305, P_{16} = 188, q_2 = 0.30902, \\ F_{17} &= 1597, n = 799, Q_{17} = 305, P_{17} = 188, q_3 = 0.19098. \end{split}$$

In this case, the value of $|Q_k|/N_k$ for large k exhibits a periodicity of p=3, indicating different values and breaking the sequence of denominators into three subsequences in the case of $\rho=1/2$.

- P. W. Anderson, Absence of diffusion in certain random lattices, Phys. Rev. 109, 1492 (1958).
- [2] L. Fleishman and P. W. Anderson, Interactions and the anderson transition, Phys. Rev. B 21, 2366 (1980).
- [3] D. Basko, I. Aleiner, and B. Altshuler, Metal-insulator transition in a weakly interacting many-electron system with localized single-particle states, Annals of Physics 321, 1126 (2006).
- [4] I. V. Gornyi, A. D. Mirlin, and D. G. Polyakov, Interacting electrons in disordered wires: Anderson localization and low-t transport, Phys. Rev. Lett. 95, 206603 (2005).
- [5] D. A. Abanin, E. Altman, I. Bloch, and M. Serbyn, Colloquium: Many-body localization, thermalization, and entanglement, Rev. Mod. Phys. 91, 021001 (2019).
- [6] W.-L. You, Z. Zhao, J. Ren, G. Sun, L. Li, and A. M. Oleś, Quantum many-body scars in spin-1 kitaev chains, Phys. Rev. Res. 4, 013103 (2022).
- [7] W.-Y. Zhang, Y.-N. Wang, D. Liu, J. Ren, J. Li, N. Wu, A. M. Oleś, and W.-L. You, Quantum many-body scars in spin-1 kitaev chain with uniaxial single-ion anisotropy, Phys. Rev. B 108, 104411 (2023).
- [8] M. Serbyn, D. A. Abanin, and Z. Papić, Quantum many-body scars and weak breaking of ergodicity, Nature Physics 17, 675 (2021).
- [9] E. van Nieuwenburg, Y. Baum, and G. Refael, From bloch oscillations to many-body localization in clean interacting systems, Proceedings of the National Academy of Sciences 116, 9269 (2019).
- [10] M. Schreiber, S. S. Hodgman, P. Bordia, H. P. Lüschen, M. H. Fischer, R. Vosk, E. Altman, U. Schneider, and I. Bloch, Observation of many-body localization of interacting fermions in a quasirandom optical lattice, Science 349, 842 (2015).
- [11] L. Dal Negro, C. J. Oton, Z. Gaburro, L. Pavesi, P. Johnson, A. Lagendijk, R. Righini, M. Colocci, and D. S. Wiersma, Light transport through the band-edge states of fibonacci quasicrystals, Phys. Rev. Lett. 90, 055501 (2003).
- [12] W. DeGottardi, D. Sen, and S. Vishveshwara, Majorana fermions in superconducting 1d systems having periodic, quasiperiodic, and disordered potentials, Phys. Rev. Lett. 110, 146404 (2013).

- [13] X. Ni, K. Chen, M. Weiner, D. J. Apigo, C. Prodan, A. Alù, E. Prodan, and A. B. Khanikaev, Observation of hofstadter butterfly and topological edge states in reconfigurable quasiperiodic acoustic crystals, Communications Physics 2, 55 (2019).
- [14] T. A. Brody, J. Flores, J. B. French, P. A. Mello, A. Pandey, and S. S. M. Wong, Random-matrix physics: spectrum and strength fluctuations, Rev. Mod. Phys. 53, 385 (1981).
- [15] J. T. Chayes, L. Chayes, D. S. Fisher, and T. Spencer, Finite-size scaling and correlation lengths for disordered systems, Phys. Rev. Lett. 57, 2999 (1986).
- [16] J.-Q. Liu and X.-B. Bian, Multichannel high-order harmonic generation from fractal bands in fibonacci quasicrystals, Phys. Rev. Lett. 127, 213901 (2021).
- [17] D. Tanese, E. Gurevich, F. Baboux, T. Jacqmin, A. Lemaître, E. Galopin, I. Sagnes, A. Amo, J. Bloch, and E. Akkermans, Fractal energy spectrum of a polariton gas in a fibonacci quasiperiodic potential, Phys. Rev. Lett. 112, 146404 (2014).
- [18] H. P. Lüschen, S. Scherg, T. Kohlert, M. Schreiber, P. Bordia, X. Li, S. Das Sarma, and I. Bloch, Single-particle mobility edge in a one-dimensional quasiperiodic optical lattice, Phys. Rev. Lett. 120, 160404 (2018).
- [19] H. Yao, T. Giamarchi, and L. Sanchez-Palencia, Lieb-liniger bosons in a shallow quasiperiodic potential: Bose glass phase and fractal mott lobes, Phys. Rev. Lett. 125, 060401 (2020).
- [20] C. Zhang, L. Sheng, and D. Xing, Topological phases induced by the aubry-andré-harper potential in the longer-range kitaev superconducting chain, Phys. Rev. B 106, 094203 (2022).
- [21] S. Weidemann, M. Kremer, S. Longhi, and A. Szameit, Topological triple phase transition in non-hermitian floquet quasicrystals, Nature 601, 354 (2022).
- [22] Z. V. Vardeny, A. Nahata, and A. Agrawal, Optics of photonic quasicrystals, Nature Photonics 7, 177 (2013).
- [23] H. Li, Y.-Y. Wang, Y.-H. Shi, K. Huang, X. Song, G.-H. Liang, Z.-Y. Mei, B. Zhou, H. Zhang, J.-C. Zhang, S. Chen, S. P. Zhao, Y. Tian, Z.-Y. Yang, Z. Xiang, K. Xu, D. Zheng, and H. Fan, Observation of critical phase transition in a generalized aubryandré-harper model with superconducting circuits, npj Quantum Information 9, 40 (2023).

- [24] P. G. Harper, The general motion of conduction electrons in a uniform magnetic field, with application to the diamagnetism of metals, Proceedings of the Physical Society. Section A 68, 879 (1955).
- [25] B.-B. Wei, Fidelity susceptibility in one-dimensional disordered lattice models, Phys. Rev. A 99, 042117 (2019).
- [26] A. Sinha, M. M. Rams, and J. Dziarmaga, Kibble-zurek mechanism with a single particle: Dynamics of the localization-delocalization transition in the aubry-andré model, Phys. Rev. B 99, 094203 (2019).
- [27] D. R. Hofstadter, Energy levels and wave functions of bloch electrons in rational and irrational magnetic fields, Phys. Rev. B 14, 2239 (1976).
- [28] J. Biddle and S. Das Sarma, Predicted mobility edges in onedimensional incommensurate optical lattices: An exactly solvable model of anderson localization, Phys. Rev. Lett. 104, 070601 (2010).
- [29] S. Das Sarma, S. He, and X. C. Xie, Mobility edge in a model one-dimensional potential, Phys. Rev. Lett. 61, 2144 (1988).
- [30] S. Das Sarma, S. He, and X. C. Xie, Localization, mobility edges, and metal-insulator transition in a class of one-dimensional slowly varying deterministic potentials, Phys. Rev. B 41, 5544 (1990).
- [31] Y. Wang, X. Xia, L. Zhang, H. Yao, S. Chen, J. You, Q. Zhou, and X.-J. Liu, One-dimensional quasiperiodic mosaic lattice with exact mobility edges, Phys. Rev. Lett. 125, 196604 (2020).
- [32] S. Ganeshan, J. H. Pixley, and S. Das Sarma, Nearest neighbor tight binding models with an exact mobility edge in one dimension, Phys. Rev. Lett. 114, 146601 (2015).
- [33] Y. Wang, J.-H. Zhang, Y. Li, J. Wu, W. Liu, F. Mei, Y. Hu, L. Xiao, J. Ma, C. Chin, and S. Jia, Observation of interactioninduced mobility edge in an atomic aubry-andré wire, Phys. Rev. Lett. 129, 103401 (2022).
- [34] F. A. An, K. Padavić, E. J. Meier, S. Hegde, S. Ganeshan, J. H. Pixley, S. Vishveshwara, and B. Gadway, Interactions and mobility edges: Observing the generalized aubry-andré model, Phys. Rev. Lett. 126, 040603 (2021).
- [35] B. Widom, Equation of State in the Neighborhood of the Critical Point, The Journal of Chemical Physics 43, 3898 (1965).
- [36] A. Szabó and U. Schneider, Non-power-law universality in onedimensional quasicrystals, Phys. Rev. B 98, 134201 (2018).
- [37] M. Thakurathi, D. Sen, and A. Dutta, Fidelity susceptibility of one-dimensional models with twisted boundary conditions, Phys. Rev. B **86**, 245424 (2012).
- [38] Y. Hashimoto, K. Niizeki, and Y. Okabe, A finite-size scaling analysis of the localization properties of one-dimensional quasiperiodic systems, Journal of Physics A: Mathematical and General 25, 5211 (1992).
- [39] S. N. Evangelou and J.-L. Pichard, Critical quantum chaos and the one-dimensional harper model, Phys. Rev. Lett. 84, 1643 (2000).
- [40] H. Hiramoto and M. Kohmoto, Scaling analysis of quasiperiodic systems: Generalized harper model, Phys. Rev. B 40, 8225 (1989).
- [41] J. C. C. Cestari, A. Foerster, M. A. Gusmão, and M. Continentino, Critical exponents of the disorder-driven superfluid-insulator transition in one-dimensional bose-einstein condensates, Phys. Rev. A 84, 055601 (2011).
- [42] C. Tang and M. Kohmoto, Global scaling properties of the spectrum for a quasiperiodic schrödinger equation, Phys. Rev. B 34, 2041 (1986).

- [43] T. Lv, T.-C. Yi, L. Li, G. Sun, and W.-L. You, Quantum criticality and universality in the p-wave-paired aubry-andré-harper model, Phys. Rev. A 105, 013315 (2022).
- [44] T. Lv, Y.-B. Liu, T.-C. Yi, L. Li, M. Liu, and W.-L. You, Exploring unconventional quantum criticality in the p-wave-paired aubry-andré-harper model, Phys. Rev. B 106, 144205 (2022).
- [45] J. Fraxanet, U. Bhattacharya, T. Grass, D. Rakshit, M. Lewenstein, and A. Dauphin, Topological properties of the long-range kitaev chain with aubry-andré-harper modulation, Phys. Rev. Res. 3, 013148 (2021).
- [46] T. Cookmeyer, J. Motruk, and J. E. Moore, Critical properties of the ground-state localization-delocalization transition in the many-particle aubry-andré model, Phys. Rev. B 101, 174203 (2020).
- [47] G. Misguich, V. Pasquier, and J.-M. Luck, Inverse participation ratios in the xxz spin chain, Phys. Rev. B **94**, 155110 (2016).
- [48] D. C. Licciardello and D. J. Thouless, Conductivity and mobility edges in disordered systems. ii. further calculations for the square and diamond lattices, Journal of Physics C: Solid State Physics 11, 925 (1978).
- [49] F. Evers and A. D. Mirlin, Anderson transitions, Rev. Mod. Phys. 80, 1355 (2008).
- [50] W.-L. You, Y.-W. Li, and S.-J. Gu, Fidelity, dynamic structure factor, and susceptibility in critical phenomena, Phys. Rev. E 76, 022101 (2007).
- [51] W.-L. You and L. He, Generalized fidelity susceptibility at phase transitions, Journal of Physics: Condensed Matter 27, 205601 (2015).
- [52] S. Chen, L. Wang, Y. Hao, and Y. Wang, Intrinsic relation between ground-state fidelity and the characterization of a quantum phase transition, Phys. Rev. A 77, 032111 (2008).
- [53] S. J. Gu, Fidelity approach to quantum phase transitions, Int. J. Mod. Phys. B 24, 4371 (2010).
- [54] D. Momeni, M. Faizal, K. Myrzakulov, and R. Myrzakulov, Fidelity susceptibility as holographic pv-criticality, Physics Letters B 765, 154 (2017).
- [55] T. LeBlond, D. Sels, A. Polkovnikov, and M. Rigol, Universality in the onset of quantum chaos in many-body systems, Phys. Rev. B 104, L201117 (2021).
- [56] B.-B. Wei and X.-C. Lv, Fidelity susceptibility in the quantum rabi model, Phys. Rev. A 97, 013845 (2018).
- [57] S. Garnerone, N. T. Jacobson, S. Haas, and P. Zanardi, Fidelity approach to the disordered quantum xy model, Phys. Rev. Lett. 102, 057205 (2009).
- [58] R. Mao, Y.-W. Dai, S. Y. Cho, and H.-Q. Zhou, Quantum coherence and spin nematic to nematic quantum phase transitions in biquadratic spin-1 and spin-2 xy chains with rhombic single-ion anisotropy, Phys. Rev. B 103, 014446 (2021).
- [59] D. Braun, G. Adesso, F. Benatti, R. Floreanini, U. Marzolino, M. W. Mitchell, and S. Pirandola, Quantum-enhanced measurements without entanglement, Rev. Mod. Phys. 90, 035006 (2018).
- [60] M. E. Fisher and M. N. Barber, Scaling theory for finite-size effects in the critical region, Phys. Rev. Lett. 28, 1516 (1972).
- [61] A. F. Albuquerque, F. Alet, C. Sire, and S. Capponi, Quantum critical scaling of fidelity susceptibility, Phys. Rev. B 81, 064418 (2010).
- [62] C. Schuster, R. A. Römer, and M. Schreiber, Interacting particles at a metal-insulator transition, Phys. Rev. B 65, 115114 (2002).